EVALUATION OF IMPACT FRACTURE TOUGHNESS OF ADHESIVELY BONDED CFRP JOINTS

Yongsik Choo[1], Sota Oshima[2], Hisayoshi Ishida[1], Takayuki Kusaka[3], Naoki Mori[3] and Tomo Takeda[4]

[1] Graduate School of Science and Engineering, Ritsumeikan University, 1-1-1, Noji-Higashi, Kusatsu, 525-8577 Shiga, Japan, gr0275vk@ed.ritsumei.ac.jp
[2] Graduate School of Engineering, Tokyo University of Agriculture and Technology, 2-24-16, Naka, Koganei, 184-8588 Tokyo, Japan, oshima@st.go.tuat.ac.jp
[3] Department of Mechanical Engineering, Ritsumeikan University, 1-1-1, Noji-Higashi, Kusatsu, 525-8577 Shiga, Japan, kusaka@se.ritsumei.ac.jp
[4] Aeronautical Technology Directorate, Japan Aerospace Exploration Agency, 7-44-1, Jindaiji, Higashimachi, Chofu 182-8522 Tokyo, Japan, takeda.tomo@jaxa.jp

Keywords: Fracture toughness, Adhesively bonded joints, Impact strength, Digital image correlation, Hopkinson bar

ABSTRACT

In this study, a novel experimental method is proposed for evaluating the nonlinear and propagation behavior of crack growth in adhesively bonded joints under impact loading using the digital image correlation (DIC) technique. Crack growth behavior could be obtained using the ψ-δ responses of subsets linearly located along the adhesive layer using the DIC technique. Consequently, mode I crack resistance curves (R-curves) could be successfully obtained under impact loading. Experimental results suggested that the mode I fracture toughness of adhesively bonded joints is affected by the mechanical properties of the adherend. The CFRP/CFRP specimen shows higher fracture toughness than the Ti/Ti specimens. The loading rate dependence of fracture toughness is also affected by the mechanical properties of the adherend. Numerical results suggest that the difference in fracture behavior between the CFRP/CFRP and Ti/Ti specimens is caused by the difference in the elastic moduli of the CFRP and Ti adherends, where the constraint of deformation in the adhesive layer is higher in Ti/Ti specimen than in the CFRP/CFRP specimen, resulting in more severe damage around the crack tip.

1 INTRODUCTION

Recently, a bonding technique using adhesive resin has become a widely used technique used in multi-material design, especially in aerospace and automotive engineering. However, the mechanical properties of polymers generally depend on various environmental factors such as temperature, humidity, or strain rate. In particular, embrittlement of the adhesive resin caused by high strain rate can lead to a reduction in fracture toughness. Therefore, numerous studies have been conducted in this field of engineering. Additionally, some experimental techniques have been developed to evaluate the fracture toughness of adhesively bonded joints at high strain rates [1]. However, difficulties still exist in dynamic fracture toughness tests at very high strain rates, owing to the effects of inertia force and kinetic energy, both on the specimen and on the measurement system [2]. The authors have proposed some experimental techniques to evaluate the debonding strength of laminated composites and adhesively bonded joints [3-6].

Critical values of energy release rate were experimentally investigated using the stress wave controlling (SWC) technique and the local strain based (LSB) formula at high strain rates for various loading modes. The SWC technique proved to be effective in reducing the effect of the inertia force, and the LSB formula proved to be effective in reducing the effect of kinetic energy on the specimen. Wedge insert fracture (WIF), end notched flexure (ENF), and mixed mode flexure (MMF) specimens were used to evaluate modes I, II, and I+II impact fracture toughness in conjunction with the split Hopkinson pressure bar (SHPB) technique. This study mainly focused on the onset strength of brittle

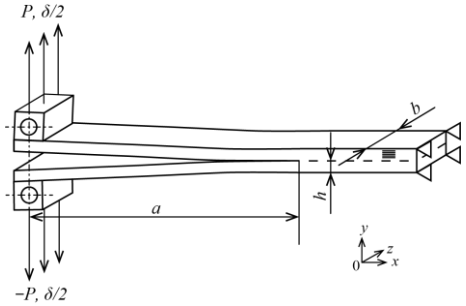

Figure 1: Schematic of a DCB specimen.

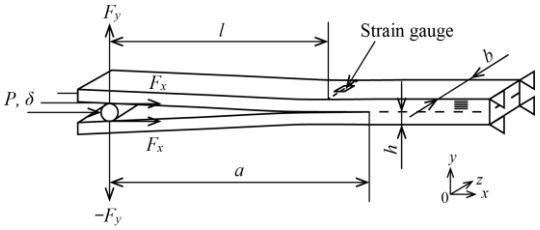

Figure 2: Schematic of a WIF specimen.

materials. Therefore, subcritical failure preceding the crack onset and propagation behavior after the crack onset were not considered. However, they should not be neglected in evaluating the fracture behavior of ductile adhesive resins that are extensively used in aerospace and automotive engineering. In this study, a novel experimental method was proposed to evaluate the nonlinear and propagation behavior of crack growth in adhesively bonded joints under impact loading using the DIC technique. Effects of loading rate and adherend properties on mode I fracture toughness were investigated using the proposed method. A numerical analysis was also conducted to study the experimental results in detail, using a finite element method (FEM) code.

2 MATERIALS AND SPECIMEN

Two types of specimens were used in this study. The first specimen was a CFRP/CFRP bonded specimen, where unidirectional T800S/3900-2B laminates of nominal thickness h = 2.66 mm were used as adherends and an epoxy-based film of nominal thickness 0.24 mm was used as the adhesive. The other specimen was a Ti/Ti bonded specimen where Ti-6Al-4V alloy plates of nominal thickness h = 1.60 mm were used as adherends and the same epoxy-based film was used as the adhesive. Figure 1 shows the DCB specimen used in static mode I fracture toughness tests at low loading rates [7]. Figure 2 shows the WIF specimen used in impact mode I fracture toughness tests at high loading rates [8]. An artificial crack was introduced in the specimen using a polymer film. The nominal width of specimen was w = 10 mm. The initial length of the artificial crack in the CFRP/CFRP specimen was a_0 = 40 mm in static DCB tests and a_0 = 40 mm in impact WIF tests. The initial length of the artificial crack in the Ti/Ti specimen was a_0 = 40 mm in static DCB tests and a_0 = 30 mm in impact WIF tests. Random patterns were painted on the side faces of the specimen to monitor the crack growth behavior using the DIC technique [9].

3 EXPERIMENTAL APPROACH

3.1 Experimental produce

Static DCB tests were performed using a universal testing machine. The displacement rate of loading point was dδ/dt = 1 mm/min. The energy release rate, G_I, was calculated using the following equations [10]:

$$G_{\mathrm{I}} = \frac{3}{2(2h)}\left(\frac{P}{b}\right)^2 \frac{\sqrt[3]{(bC)^2}}{\alpha} \tag{1}$$

$$\frac{a}{2h} = \alpha\sqrt[3]{bC} + \beta \tag{2}$$

where P is the load applied to the specimen, δ is the displacement of the loading point, and C (= δ/P) is the loading point compliance of the specimen. α and β are constants that depend upon on the elastic properties of the specimen. The crack length of the specimen, a, is defined as the horizontal

distance of the crack tip from the loading line. Impact DCB tests were performed using a SHPB system as shown in Figure 3 [3]. The displacement rate of loading point was dδ/dt = 8 m/s. The energy release rate, G_I, was calculated using the following equations [8]:

$$G_{\mathrm{I}} = \frac{3A^2}{2(2h)}\left(\frac{\varepsilon_{\mathrm{h}}}{bD^*}\right)^2 \frac{\sqrt[3]{(bC^*)^2}}{\alpha}; \quad A = \frac{(a+e)l^*}{(a^*+e)l} \tag{3}$$

where ε is the surface strain near the crack tip and D (= ε/F_y) is the strain coefficient of the specimen, which was determined by a calibration test prior to impact WIF [8].

l is the horizontal distance of the gauge position of the surface strain, ε, from the crack tip. a*, l*, C* and D* are the crack length, gauge position, compliance and strain coefficient in the calibration test, respectively. e (= -β(2h)) is the correcting factor of crack length [10]. The strain rate dependence of the elastic properties of the specimen was assumed to be negligible in this study.

3.2 Crack Growth Measurement

A high-speed digital video system was employed to monitor the crack growth behavior in the specimens as shown in Figure 3. The sampling rate of the camera was set to 30,000 frames per second and the output signal from the strain gauges, G_1, was utilized as the trigger for sampling. The deformation field of adhesive layer was investigated using several pairs of measurement points (subsets), which were virtually defined on the side faces of upper and lower adherends using the DIC technique, as shown in Figure 4. In the WIF specimen, the crack length, a, and the gauge position, *l*, can be defined by the initial crack length, a_0, initial gauge position, l_0, displacement of loading point, δ, and crack extension, Δa, as follows:

$$a = a_0 - \delta + \Delta a \tag{5}$$

$$l = l_0 - \delta \tag{6}$$

It should be noted that the crack length, a, and the gauge position, *l*, are dependent on the displacement, δ, even if the crack is stationary, Δa = a.

Figure 5 shows the relative displacement of two subsets located in the forward region (uncracked region) ahead of the the crack tip, obtained using the DIC technique in a static DCB test. The abscissa represents the displacement of loading point, δ. The ordinate represents the relative displacement, ψ,

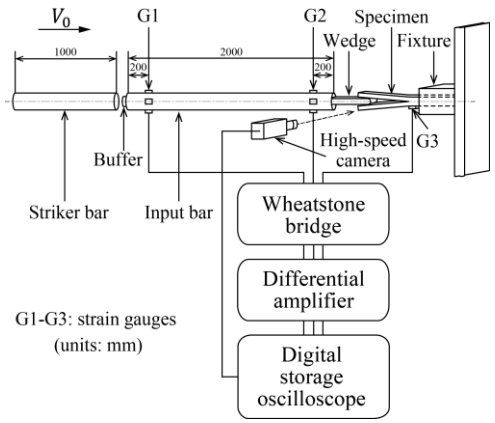

Figure 3: Experimental setup of impact WIF test.

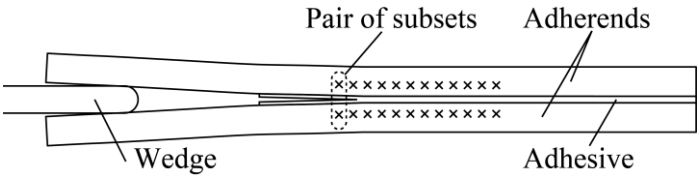

Figure 4: Arrangement of subsets.

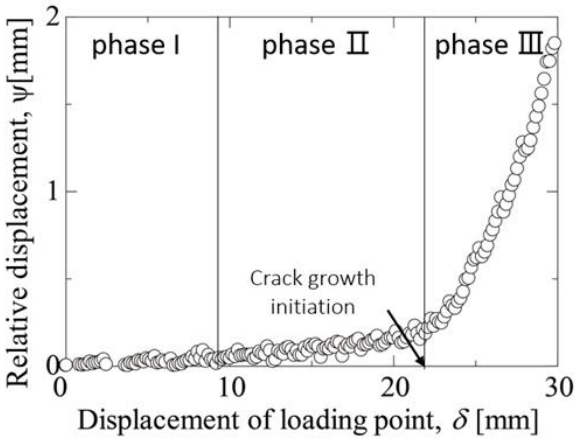

Figure 5: Relative subset distance compared to opening displacement of loading point

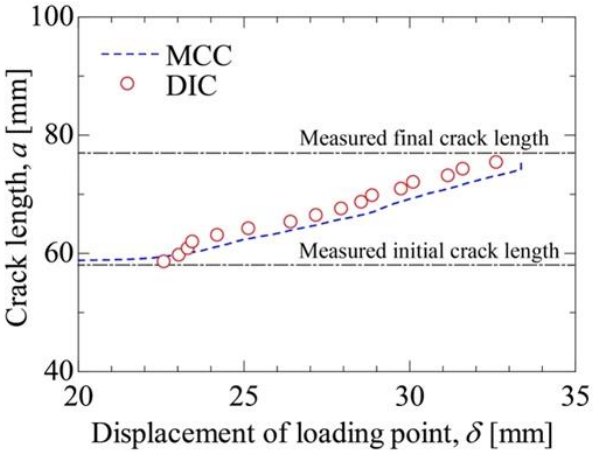

Figure 6: Crack length estimated from compliance and proposed method

between the subsets defined on the upper and lower adherends. As shown in the figure, the relative displacement, ψ, increased with increasing the displacement, δ, where the ψ-δ response could be divided into three parts, phase I, II and III. In phase I, the relative displacement, ψ, was almost zero regardless of the displacement, δ. In this region, the strain field around the subsets was not affected by the crack tip stress field. In phase II, the relative displacement, ψ, gradually increased with an increase in the displacement, δ. In this region, the strain field around the subsets was affected by the crack tip stress field due to plastic deformation. In phase III, the relative displacement, ψ, steeply increased with an increase in the displacement, δ. In this region, the crack passed the horizontal position of the subsets. Additionally, the relative displacement, ψ, can be considered to be equal to the crack opening displacement at the subset position.

Figure 6 shows the crack growth behavior in a static DCB test. The abscissa represents the displacement of the loading point, δ. The ordinate represents the crack length of the specimen, a. In Figure 5, the red circles show the results obtained using the DIC technique, where the crack growth behavior was determined from the border of phases II and III. The blue dashed line shows the results obtained from the modified compliance calibration (MCC) technique, where the crack growth behavior was determined from the compliance of the loading point, using Equation 2. The black dotted lines show the actual crack length directly measured by the liquid penetrant examination. As shown in Figure 6, the DIC technique resulted in higher accuracy than MCC in direct measurements. The above results suggest that crack growth behavior could be obtained using the ψ-δ responses of subsets linearly located along the adhesive layer, using the DIC technique. Consequently, mode I crack resistance curves (R-curves) could be successfully obtained under impact loading, as shown in the next section.

3.3 Mode I Fracture Toughness

Figure 7 shows the R-curves at low loading rates obtained from the static DCB tests. The abscissa represents the crack extension, Δa. The ordinate represents the fracture toughness, G_{IC}. The blue line shows the result for the CFRP/CFRP specimen, where the solid and dashed lines represent the stable

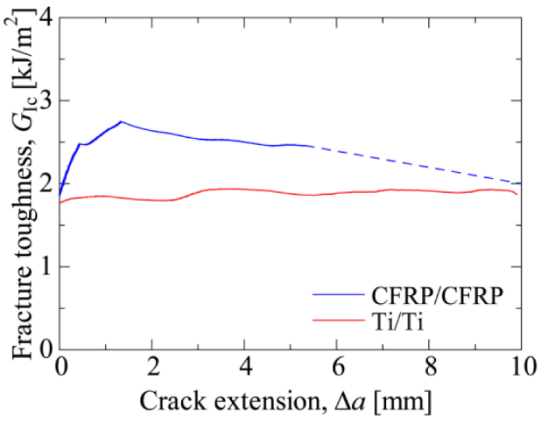

Figure 7: R-curves from static DCB test

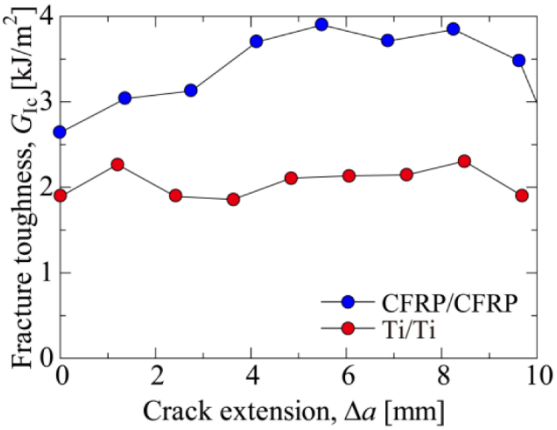

Figure 8: R-curves from impact WIF test

and unstable crack growth, respectively. The red line shows the result of the Ti/Ti specimen, where only the stable crack growth was observed. As shown in the figure, the fracture toughness, G_{IC}, slightly decreased with crack growth in the CFRP/CFRP specimens, where the cohesive failure of adhesive layer was observed in the stable region but the interlaminar failure of adherend was observed in the unstable region. However, the fracture toughness, G_{IC}, was almost constant in the Ti/Ti specimens, where only the cohesive failure was observed. In addition, the fracture toughness, G_{IC}, of the CFRP/CFRP specimen was significantly higher than that of the Ti/Ti specimen.

Figure 8 shows the R-curves at high loading rates obtained from the impact WIF tests. The abscissa represents the crack extension, Δa. The ordinate represents the fracture toughness, G_{IC}. The blue circles show the result of the CFRP/CFRP specimen, where the cohesive failure of adhesive layer was observed during the early stage of crack growth but the interlaminar failure was observed subsequently. The red circles show the result for the Ti/Ti specimen, where only the cohesive failure of adhesive layer was observed. As shown in the figure, the fracture toughness, G_{IC}, increased with crack growth in the CFRP/CFRP specimens, which differed from the tendency observed in static DCB tests. However, the fracture toughness, G_{IC}, was almost constant in the Ti/Ti specimens, which was similar tendency observed in static DCB tests.

Comparison of the results in Figures 7 and 8 shows that the fracture toughness, G_{IC}, increased with loading rate in the CFRP/CFRP specimen, whereas it was approximately independent of loading rate in the Ti/Ti specimen. These results suggest that the mode I fracture toughness of adhesively bonded joints was affected by the mechanical properties of adherend; The CFRP/CFRP specimen showed higher fracture toughness than the Ti/Ti specimens. The loading rate dependence of fracture toughness was also affected by the mechanical properties of adherend.

4 NUMERICAL APPROACH

4.1 Numerical procedure

Finite element analyses of the DCB specimens were carried out to study the effect of the mechanical properties of the adherend on the fracture behavior of adhesively bonded joints. A finite element code, MARC 2013™, was used for the analyses. The updated Lagrangian formulation was employed for considering the nonlinear behavior caused by the plastic deformation of the adhesive layer and large displacement of the specimen. The Gurson model was also employed to consider the damage under the triaxial stress field in the adhesive layer.

Gurson's yield function can be given by the following equation [11-13].

$$F = \left(\frac{\sigma_{eq}}{\sigma_0}\right)^2 + 2q_1 f \cosh\left(\frac{q_2 \sigma_{kk}}{2\sigma_0}\right) - [1 - (q_1 f)^2] = 0$$

where σ_{eq} and σ_{kk} are the global equivalent stress and hydrostatic stress. σ_0 is the matrix flow stress. q_1 and q_2 are the Tvergaard correction coefficients. f is the void volume fraction.

4.2 Numerical Results

The distribution of the void volume fraction near the crack tip in the CFRP/CFRP and Ti/Ti specimen obtained using finite element analyses are shown in Figures 9 and 10, respectively. The abscissa represents the distance from the crack tip, x. The ordinate represents the void volume fraction, f, on the midplane of the adhesive layer. The black, red, blue, and green lines show the results at GI = 0.5, 1.0, 1.5, and 2.0 kJ/m^2, respectively. As shown in the figures, the void volume fraction, f, increased with an increase in the energy release rate, G_I. However, the values of f at the same x and G_I were larger in the Ti/Ti specimen than in the CFRP/CFRP specimen. In particular, the maximum values of f at $x = 0$ were larger in the Ti/Ti specimen than in the CFRP/CFRP specimen, suggesting that the crack growth occurs at lower value of G_I in the Ti/Ti specimen than in the CFRP/CFRP specimen.

The aforementioned results agreed with the experimental tendencies shown in Figures 7 and 8. The difference in fracture behavior between the CFRP/CFRP and Ti/Ti specimens was caused by the difference in the elastic moduli of the CFRP and Ti adherends, where the constraint of deformation in adhesive layer was higher in the Ti/Ti specimen than in the CFRP/CFRP specimen, resulting in more severe damage around the crack tip.

5 CONCLUSIONS

A novel experimental method was proposed for evaluating the nonlinear and propagation behavior of crack growth in adhesively bonded joints under impact loading, using the DIC technique. Effects of the loading rate and adherend properties on mode I fracture toughness was investigated using the proposed method. A numerical analysis approach was also conducted to study the experimental results in detail using an FEM code. The results can be summarized as follows:

(1) Crack growth behavior could be obtained using the ψ-δ responses of subsets linearly located along the adhesive layer, through the DIC technique. Consequently, mode I crack resistance curves (R-curves) could be successfully obtained under impact loading.
(2) The mode I fracture toughness of adhesively bonded joints was affected by the mechanical properties of the adherend; The CFRP/CFRP specimen showed higher fracture toughness than the Ti/Ti specimens.
(3) The loading rate dependence of fracture toughness was affected by the mechanical properties of the adherend
(4) The difference in fracture behavior between the CFRP/CFRP and Ti/Ti specimens was caused by the difference in the elastic modulus between the CFRP and Ti adherends. The constraint of deformation in adhesive layer was higher in the Ti/Ti specimen than in the CFRP/CFRP specimen, resulting in more severe damage around the crack tip.

ACKNOWLEDGEMENTS

This research was supported by Japan Aerospace Exploration Agency. We thank our colleagues from Ritsumeikan University who provided insight and expertise that greatly assisted the research.

REFERENCES

[1] B.R.K. Blackman, A.J. Kinloch, F.S. Rodriguez-Sanchez and W.S. Teo, The fracture behaviour of adhesively-bonded composite joints: Effects of rate of test and mode of loading, *International Journal of Solids and Structures*, **49**, 2012, pp. 1434-1452
[2] F. Sugiyama and K. Ogawa, A New Application of Split-Hopkinson Bar to Impact Bending Test on Advanced Brittle Materials, *Plasticity and Impact Mechanics*, 1996, pp.446-483
[3] H. Kolsky, Stress Waves in Solid, Chap. 4, Dover. 1963.

[4] W. Chen and B. Song, Split Hopkinson (Kolsky) Bar: Design, Testing and Application, Chap. 1, 2, Springer, 2011
[5] W.G. Knauss, K. Ravi-chandar, Some basic problems in stress wave dominated fracture, International Journal of Fracture, 27, 1985, pp. 127-143.
[6] A.A Bezemer C.B. Guyt and A. Vlot, New Impact Specimen for Adhesives: Optimization of High-Speed-Loaded Adhesive Joints, *International Journal of Adhesion and Adhesives*, **18**, 1998, pp. 255-260
[7] O'Brien, T.K., Characterization of Delamination Onset and Growth in a Composite Laminate, Damage in Composite Materials, *ASTM STP 775*, 1982, pp. 140-167.
[8] T. Kusaka, M. Hojo, Y.W. Mai, T. Kurokawa, T. Nojima and S. Ochiai, Rate dependence of mode I fracture behaviour in carbon-fibre/epoxy composite laminates, *Composites Science and Technology*, **58**, 1998, pp.591-602
[9] Oshima, S., Ishida, H., Tanegashima, R., Kusaka, T., Takeda, T., Experimental Characterization of Crack Growth Behavior in Adhesive Interface under Impact Loading, *Key Engineering Materials*, **715**, 2016, pp. 116-121.
[10] Hojo, M., Kageyama, K. and Tanaka, K., Prestandardization Study on Mode I Interlaminar Fracture Toughness Test for CFRP in Japan, *Composites*, **26**, 1995, pp. 243-255.
[11] A.L. Gurson, Continuum Theory of Ductile Rupture by Void Nucleation and Growth: Part I—Yield Criteria and Flow Rules for Porous Ductile Media, *Journal of Engineering Materials and Technology*, **99**, 1977, pp. 2-15
[12] V. Tvergaard and A. Needleman, Analysis of the cup-cone fracture in a round tensile bar, *Acta Metallurgica*, **32**, 1984, pp. 157-169
[13] T. Ikeda, J. Mano, D. Ikemoto, DB. Lee and N. Miyazaki, Constraint effect of adherends on the fracture of adhesive joint, *Transactions of the Japan Society of Mechanical Engineers*, Part A. **69**, (2), 2003, pp. 434-441 (In Japanese)

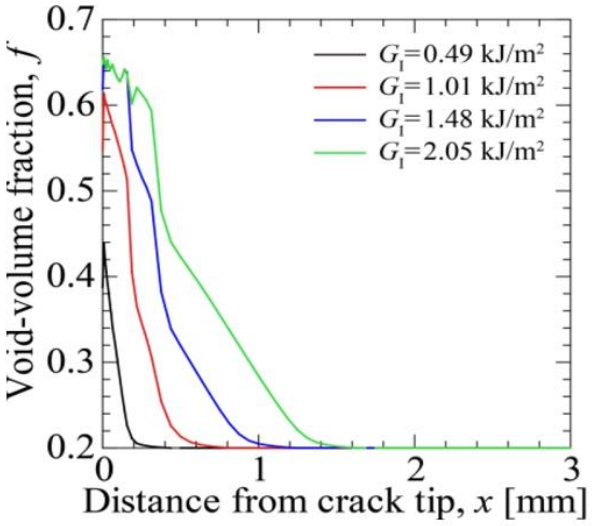

Figure 9: FEM result of CFRP

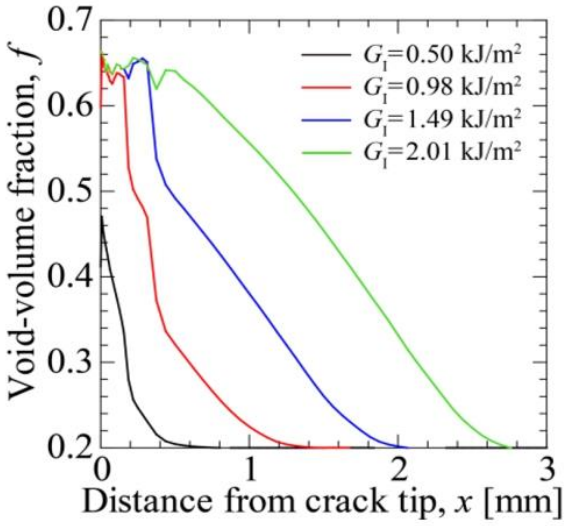

Figure 10: FEM result of Titanium